10

Modelling drape deformation of woven fabrics and garments – computation and simulation

10.1 Introduction

Due to its inherent extreme thinness and high flexibility, the drape deformation of a fabric sheet usually involves only very small strains even under very large deflections; most of these come from bending and only a small amount is due to in-plane stretching. As a result, a fabric sheet can still retain its original surface area and volume after drape deformation. For this reason, the finite-volume method is reasonably appropriate for simulating fabric drape deformation. In Chapter 9, the theoretical analysis of this method was developed, and in this chapter a detailed computational evaluation of the model is reported whereby its predictability and accuracy can be confirmed. In addition, a B-spline method is used to map fabric texture and colours to a three-dimensional draped garment.

10.2 Computation

The analysis starts with an initially flat fabric sheet which has been discretised into r control volumes. For a three-dimensional problem, the unknown vector $\boldsymbol{X}$ in equation 9.14 contains $3r$ co-ordinate vector components, i.e. the degrees of freedom of the problem are $3r$. The computational procedure including the line-search technique for a three-dimensional problem is as follows:

(1) Set up the initial grid and calculate the initial three-dimensional co-ordinates of all grid nodes.
(2) Calculate the nodal forces due to gravity and external loading (if any) and form the total load vector $\boldsymbol{R}$.
(3) Begin iterative loops: steps (4)–(14).
(4) Check if the grid node to be dealt with is an internal node or a boundary node.
(5) Form the element internal force vector, with appropriate different treatments for internal and boundary grid nodes.

(6) Form the element tangent stiffness matrix, with appropriate different treatments for internal and boundary grid nodes.
(7) Form the global internal force vector $\boldsymbol{F}$, the global tangent stiffness matrix $\boldsymbol{K}$ and the out-of-balance force vector $\boldsymbol{G} = \boldsymbol{F} - \boldsymbol{R}$.
(8) Calculate the old position vector at each grid node Δ^{old}.
(9) Impose the boundary conditions.
(10) Apply Crout factorisation to the tangent stiffness matrix $\boldsymbol{K}$ and then solve the first part of equation (9.14) to obtain the incremental co-ordinate vector $\Delta\boldsymbol{X}$.
(11) Compute the new co-ordinate vector $\boldsymbol{X}^{\text{new}} = \boldsymbol{X}^{\text{old}} + \Delta\boldsymbol{X}$.
(12) If necessary, carry out line searches to obtain an iterative step length η and then the updated co-ordinate vector $\boldsymbol{X}^{\text{update}} = \boldsymbol{X}^{\text{old}} + \eta\Delta\boldsymbol{X}$, otherwise go to step (13). The line search procedure (Crisfield, 1997) is as follows:

(i) Compute $s_0 = s(\eta = 0) = \Delta\boldsymbol{X}^{\text{T}}(\boldsymbol{F}^{\text{old}} - \boldsymbol{R})$. If it is positive, set $\eta = 1$ and go to step (13).
(ii) Set $\eta^{(1)} = 0$, $\eta^{(2)} = 1$ and $\eta = \eta^{(2)}$.
(iii) Compute $s(\eta) = \Delta\boldsymbol{X}^{\text{T}}(\boldsymbol{F} - \boldsymbol{R}) = \Delta\boldsymbol{X}^{\text{T}}g(\eta)$.
(iv) Check if the equation $|r_{\text{ls}}| = |s(\eta)/s_0| < \beta_{\text{ls}}$ is satisfied or the maximum or minimum allowed step length has been reached twice. If either condition is met, go to step (13).
(v) Find the step length η_- which is the minimum of all previously obtained step lengths with a negative ratio $r_{\text{ls}-}$. If such a step length does not exist, go to step (viii).
(vi) Find the step length η_+ which is the maximum of all previous step lengths with a positive ratio $r_{\text{ls}+}$ and is at the same time smaller than η_-
(vii) Calculate the new step length using the following linear interpolation:

$$\eta = \frac{r_{\text{ls}-} \cdot \eta_+ - r_{\text{ls}+} \cdot \eta_-}{r_{\text{ls}-} - r_{\text{ls}+}}$$

(viii) If the calculated step length $\eta > \eta_+ + 0.2(\eta_- - \eta_+)$, set $\eta = \eta_+ + 0.2(\eta_- - \eta_+)$ and go to step (x).
(ix) Calculate the new step length using a linear extrapolation between the current and previous step lengths.
(x) If the step length from (viii) $\eta > \alpha_{\text{ls}}\eta_{\text{maxp}}$, set $\eta = \alpha_{\text{ls}}\eta_{\text{maxp}}$, where α_{ls} is a predefined maximum amplification factor and η_{maxp} is the maximum of all previous step lengths.
(xi) Calculate the updated co-ordinate vector $\boldsymbol{X}^{\text{update}} = \boldsymbol{X}^{\text{old}} + \eta\Delta\boldsymbol{X}$.
(xii) If the maximum number of line searches has not been reached, return to step (iii), otherwise go to step (13).

(13) Calculate the updated position vector at each grid node Δ^{update}.

(14) Convergence is checked by evaluating the iterative change of the position vector at each grid node using equation 9.22. If $\beta \leq \beta_d$ is satisfied at all grid nodes, convergence is deemed to have been achieved; otherwise more iterations need to be carried out.

(15) If convergence has not been achieved and the maximum number of iterations specified at the beginning of the problem has not been reached, return to step (4), otherwise stop.

10.3 Two-dimensional drape simulations

10.3.1 Cantilever cloth strips

Numerical simulations using two-dimensional drape deformations of cloth cantilever strips are presented first. The simulations are for two cloth strips made of the same wool fabric, with their long directions along either the warp or the weft directions. These cloth strips have been experimentally studied before (Kang and Yu, 1995) where their mechanical properties were determined using the KES tester (Kawabata, 1975). The Poisson's ratio is assumed to be zero in the present study here and in all subsequent calculations. Both cloth strips are 5 cm long and 1 cm wide. A mesh with 56 grid nodes (or control volumes) was used in the simulations (Fig. 10.1a). The numerical results for fabric cantilevers were obtained using the full Newton–Raphson method without line searches as they were found not to be very useful for these cases.

10.3.2 Deformed shapes

The predicted deflected shapes and the corresponding experimental data (Kang and Yu, 1995) for the two strips are shown in Fig. 10.1b A close match in the draped shapes is evident.

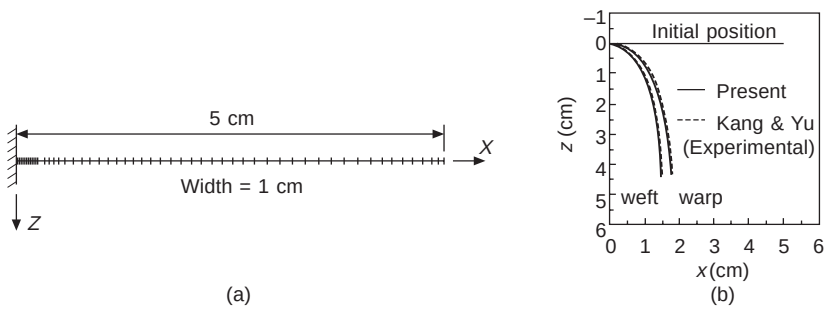

10.1 Fabric cantilevers: (a) geometry and mesh; (b) deflection curves.

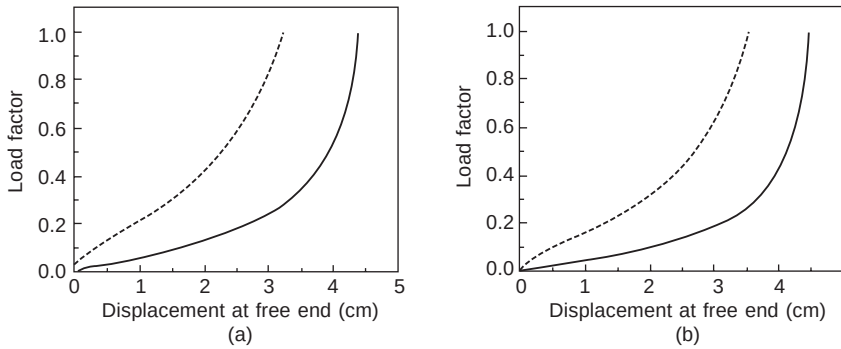

10.2 Load–displacement curves of fabric cantilevers: (a) warp direction; (b) weft direction. (Solid line = vertical displacement (w); dotted line = horizontal displacement ($-u$).)

10.3.3 Load–displacement curves

As discussed earlier, in conventional non-linear finite-element analysis of load-bearing structures, the step-by-step incremental approach is widely employed for solving the non-linear algebraic equations. As this method has also been popular in finite-element modelling of fabric deformations, it is of interest to examine the relative efficiency of the single-step full Newton–Raphson method adopted here and the incremental iterative method.

In the incremental iterative approach, the self weight of the fabric is seen as external loading and is applied to the fabric strip step-by-step. Figure 10.2 shows the load–displacement curves of the free end of the two fabric cantilevers obtained using a 50-step incremental iterative procedure, where the vertical axis represents the load factor with the self weight as the reference load. The calculated final deflection curves for the fabric strips are identical to those presented in Fig. 10.1b. The required computer time on a Pentium® II/266 personal computer for each simulation without line searches is listed as follows:

- 50-step: warp direction 8.35 seconds and weft direction 5.77 seconds;
- single-step: warp direction 0.39 seconds and weft direction 0.38 seconds.

Although variations in the control parameters of the incremental solution procedure may make it more efficient, the large difference in computer time makes it clear that the method adopted here is more efficient.

In all previous finite-element simulations of drape deformations, even though the step-by-step solution procedure was used, the load–displacement curves were seldom plotted. This is understandable since the result which is of practical interest is the final deformed shape. However, the shape of a load–displacement curve has much bearing on the success of a particular incremental solution procedure, so beneficial insight may be gained by plotting

some load–displacement curves. It was necessary to plot the load–displacement curves of the wool cantilevers here in order to explain the inefficiency of the 50-step approach. These load–displacement curves are of a geometrically stiffening type. Similar curves have been obtained for three-dimensional draping of fabrics by Kim (1991). This kind of curve is believed to be typical of fabric drape deformations as fabric sheets transform themselves from a bending deformation-dominant structure into a stretching deformation-dominant membrane during the draping process. The behaviour is highly non-linear in the initial stage of loading and then becomes more linear as deformations progress. A great deal of computer time may thus be consumed in tracing the early part of the load–displacement curve in a step-by-step solution process, although information on this part of the deformation is of no practical value in real fabric drape simulations. The single-step approach is thus more rational and efficient.

There may be concern that the single-step procedure could lead to a different final state from that determined by a step-by-step solution process if the solution is non-unique. A number of the problems studied below were checked by running the analysis using a step-by-step solution procedure and the same final shape was reached.

10.3.4 Convergence of the grid scheme

So far, the issue of convergence of the solution as the grid is refined has not been mentioned. This is considered here for the wool cantilever strip bent in the warp direction. The results are given in Table 10.1, where solutions in terms of the free end displacements are compared for different uniform discretisation schemes. It is seen that a coarse grid leads to a softer structure, and the solution converges towards the exact solution as more grid nodes are employed. Compared to the rate of convergence of a uniform grid, a non-

Table 10.1 Displacements at the free end of a fabric cantilever (warp-direction)

Uniform grid	**Horizontal displacement $-u$ (cm)**	**Vertical displacement w (cm)**
5×1	3.6132	4.6698
10×1	3.4798	4.5551
20×1	3.3763	4.4671
40×1	3.3100	4.4109
80×1	3.2825	4.3791
160×1	3.2527	4.3623
320×1	3.2270	4.3537
Non-uniform grid 56×1	3.2437	4.3552
Non-uniform grid 112×1	3.2395	4.3506

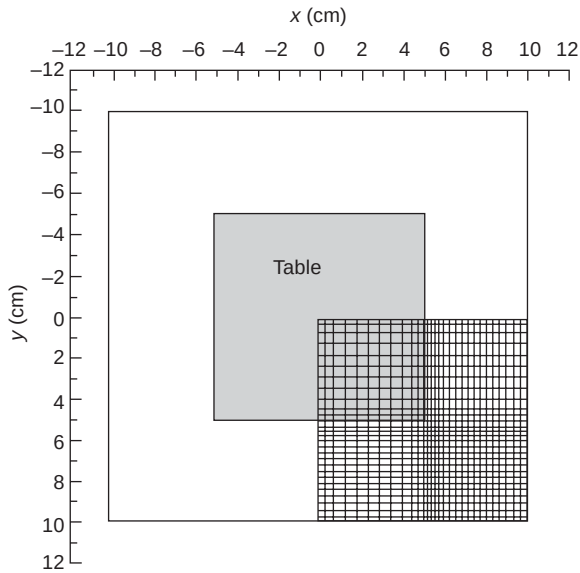

10.3 A non-uniform grid scheme for a square fabric sheet draped over a square table.

uniform grid as employed above (Fig. 10.3) proves to be much more effective for this problem. Doubling the grid density of the non-uniform grid employed above (56×1) leads to few differences (Table 10.1), indicating that the results from the 56×1 grid are accurate. The issue of grid convergence is not further discussed in this section, but all the grid schemes employed for the examples in this section are good enough to give accurate predictions.

10.4 Three-dimensional drape simulations

10.4.1 General

In this section, a number of three-dimensional drape simulations are presented. They are all initially flat and have a square undeformed shape. All numerical simulations were carried out on a Pentium® II/266 personal computer.

10.4.2 Square fabric sheet concentrically draped over a square table

The case of a square fabric sheet with a width of 20 cm concentrically draped over a 10 cm $\times$ 10 cm square table is considered here. Since both the geometry and the material properties are doubly symmetric about the axes of symmetry, only a quarter of the fabric sheet was modelled in the numerical analysis. Figure 10.4 shows the mesh used which features a non-uniform grid of

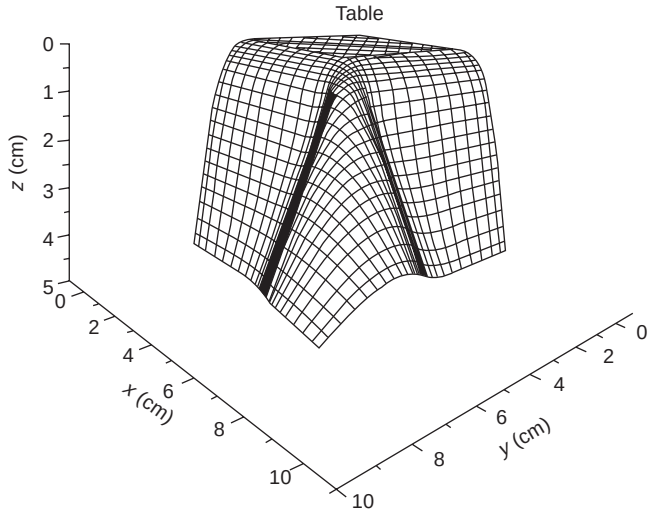

10.4 Shape of a fabric sheet draped over a square table.

31 × 31 nodes (or control volumes) adopted for the numerical simulation. The grid was finer near the edges of the table to cater for the more complex deformations here. The nodes which are in contact with the table were fixed in all directions.

Figure 10.4 shows the three-dimensional draped shape of the fabric sheet, while Fig. 10.5 shows its projection onto the horizontal (or *x*–*y*) plane. The

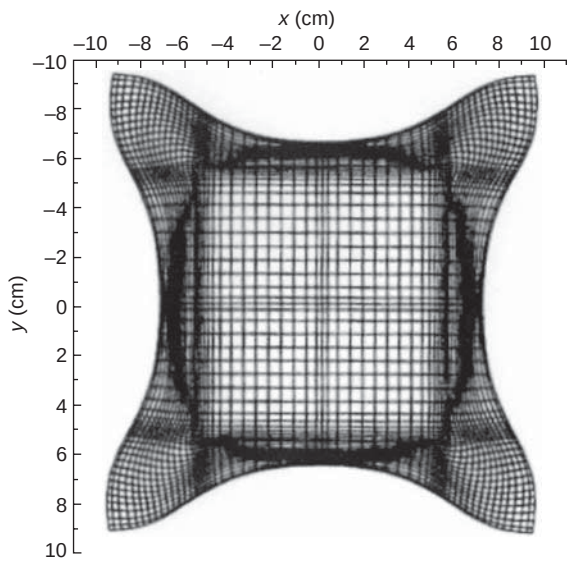

10.5 Horizontal projection of a fabric sheet draped over a square table.

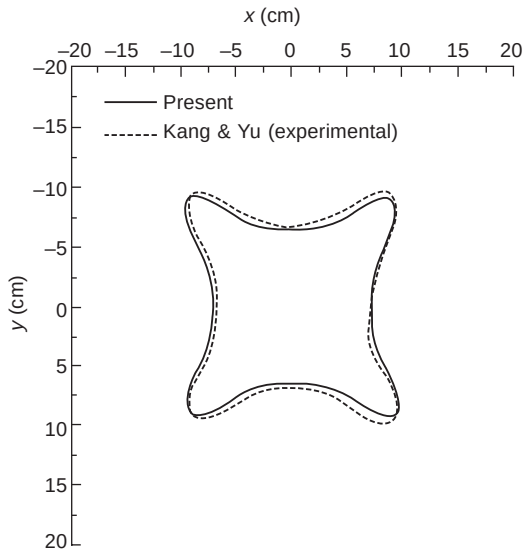

10.6 Draped shape of a fabric sheet: comparison between theoretical prediction and experiment.

projected image is compared in Fig. 10.6 with the experimental measurements given by Dhande *et al*. (1993). It is clear from Fig. 10.6 that the predicted draped shape matches the experimental result quite well. This further demonstrates the validity of the proposed method.

It has been found that previous authors often gave qualitative information (e.g. the appearance of the draped cloth sheet) rather than precise quantitative information when carrying out comparisons or presenting results. This makes precise numerical comparisons difficult, although such comparisons are important in verifying numerical results. Table 10.2 thus provides the final co-ordinates of the nodal points located on the two edges of the quarter model of the wool fabric sheet. These results should be useful as benchmark results for comparisons with predictions from other numerical methods.

10.4.3 Square fabric sheet eccentrically draped over a square table

To evaluate the model, a 15 cm × 15 cm fabric sheet eccentrically draped over the corner of a square table was also analysed. The area of the table corner in contact with the cloth is 7.5 cm × 7.5 cm and a non-uniform grid was adopted for the initially flat fabric sheet (Fig. 10.7). Again, the portion of the fabric sheet lying on the table was prescribed to have no displacements during the deformations. The predicted three-dimensional deformed shape using a 31 × 31 grid is given in Fig. 10.8.

Table 10.2 Co-ordinates of edge points on the wool fabric sheet before and after deformations

Point No.	Initial co-ordinates ($z = 0$)		Co-ordinates after deformations		
	x	***y***	***x***	***y***	***z***
1	0.0	10.0	0.0000	6.5289	4.5662
2	2.5	10.0	2.4892	6.7319	4.5169
3	5.0	10.0	4.8289	7.5258	4.2028
4	7.5	10.0	6.9641	8.7134	3.6763
5	10.0	10.0	9.3813	9.2186	3.6625
6	10.0	7.5	9.3281	6.8742	3.0236
7	10.0	5.0	8.2324	4.7471	3.7170
8	10.0	2.5	7.3465	2.4851	4.2436
9	10.0	0.0	7.1206	0.0000	4.3385

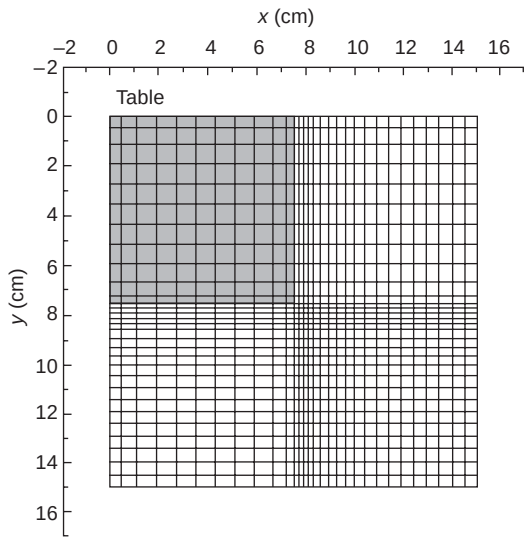

10.7 A non-uniform grid scheme for a fabric sheet eccentrically draped over a table.

10.4.4 Square fabric sheet supported at two diagonal corners

A numerical simulation was also carried out for the drape deformations of an initially flat square fabric sheet 15 cm × 15 cm in size fixed at two diagonal corners. A uniform grid scheme of 41 × 41 nodes was used in the simulation. The final draped shape predicted is shown in Fig. 10.9.

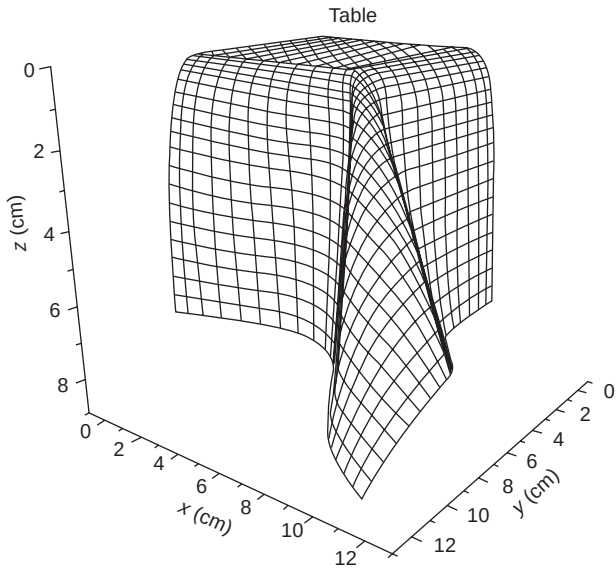

10.8 Shape of a fabric sheet eccentrically draped over a table.

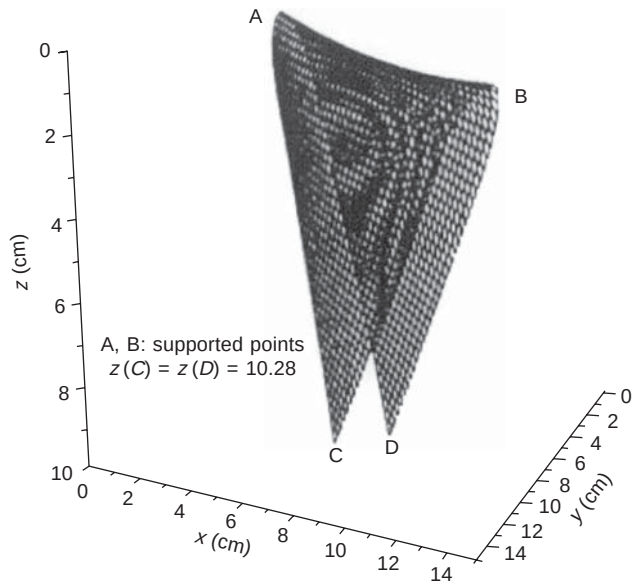

10.9 Draped shape of a fabric sheet supported at diagonal corners.

10.5 Fabric buckling simulation

Wrinkles often appear in cloth products in daily use. The phenomenon of wrinkle formation is one of buckling and post-buckling deformations in

terms of structural mechanics. Wrinkles appear easily because fabric sheets are very flexible in bending and can easily buckle when compressive stresses arise. It is therefore of interest to examine the ability of the model to simulate buckling and post-buckling deformations in fabric sheets.

Suppose that a square fabric piece is placed on a flat surface and a pair of pulling forces is exerted in the plane of the fabric surface on the two diagonal corners, one may be able to intuitively expect that out-of-plane deformations will arise. This kind of deformation can also be confirmed using simple experiments. The reason for the appearance of out-of-plane deformations is the non-uniformity of the applied stretching, which leads to compressive membrane stresses in the perpendicular direction. Consequently, wrinkles will appear unless the applied forces are very small. The following numerical simulations were conducted to capture this type of post-buckling deformation phenomenon.

The fabric considered here is a pure wool fabric with the properties of wool material. The fabric sheet is 15 cm $\times$ 15 cm, modelled by a 31 $\times$ 31 grid. As the fabric sheet is assumed to be lying on a table, the gravitational forces were assumed to be balanced by reactions from the table and were neglected in the analyses. The top left corner was prevented from any in-plane displacements and the top right corner was prevented from any horizontal displacement. These in-plane restraints were specified to avoid rigid body motions. In addition, the fabric sheet was supported vertically around its edge. The applied pulling force is 50 gf (1 gf = 0.0098 N).

Under these idealised conditions, the problem is a typical plane-stress problem and the model can predict only in-plane deformations (Fig. 10.10). However, it is recognised that the equilibrium state predicted by the model is not a stable one if the applied force is sufficiently large, and there exist other more stable equilibrium positions as discussed above.

In order to find the more stable post-buckling state, a small perturbation force was applied to the fabric sheet during the simulation. The perturbation force used was a small concentrated force at the centre of the fabric sheet in the negative direction of the z co-ordinate (upwards). Interestingly, different deformation modes were obtained depending on the amount of perturbation force (Fig. 10.11). When the perturbation force Q_p is below 7.795×10^{-5} gf, the deformed shape assumes a wavy pattern (Fig. 10.11a). With a slightly higher perturbation force ($Q_p = 7.800 \times 10^{-5}$ gf), the deformed shape assumes a roughly asymmetric shape about the stretched diagonal, featuring one major crest and one major trough. As the perturbation force is increased further, this asymmetric pattern gradually transforms into a roughly symmetric pattern (Figs 10.11c–h). The deformed shape is close to symmetric when the perturbation force is greater than 0.5 gf and features a single major crest.

These deformed shapes deserve further investigation and verification from other researchers in the future. In particular, the shape shown in Fig. 10.11a

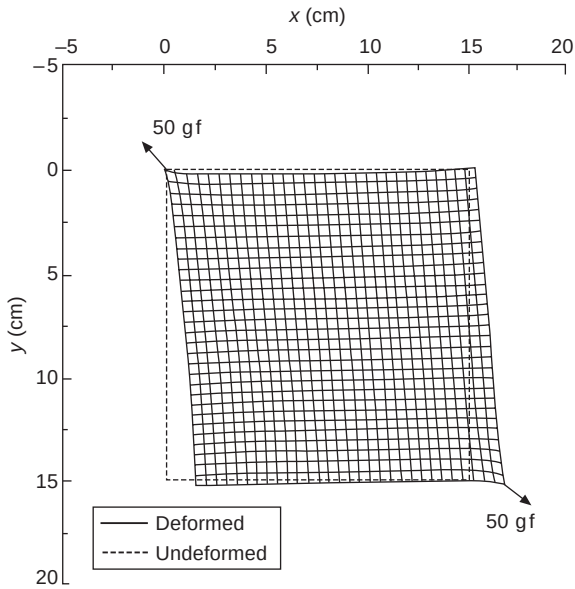

10.10 In-plane deformations of a fabric sheet under diagonal tension.

is difficult to produce by doing a simple experiment with a piece of cloth on a table. The shapes shown in Figs 10.11b–h appear to be obtainable in a simple experiment by appropriately perturbing the fabric cloth so that it is guided into the appropriate mode. These shapes (Figs 10.11b–h) have a clear load-path across the loaded diagonal and appear to be stable. The first mode shown in Fig. 10.11a may be one which needs such a small disturbance that it cannot be achieved in a simple experiment, although more elaborate experiments may prove otherwise. In addition, the conditions assumed in the numerical simulations are not exactly the same as those of a fabric sheet resting on a table under diagonal pulling. Explanations aside, these different modes do show that fabric deformations may be dependent on small perturbations.

10.6 Circular fabric sheets over circular pedestals

Numerical simulation of two circular sheets of different sizes made of two different fabrics (fabric A and fabric B) are presented in this section. The Poisson's ratio is taken as zero for both fabrics in the simulations.

10.6.1 Drape behaviour of a circular fabric sheet A

The circular fabric sheet made of fabric A is referred to as fabric sheet A and is considered first. The radius of the sheet is 12.7 cm, and that of the supporting

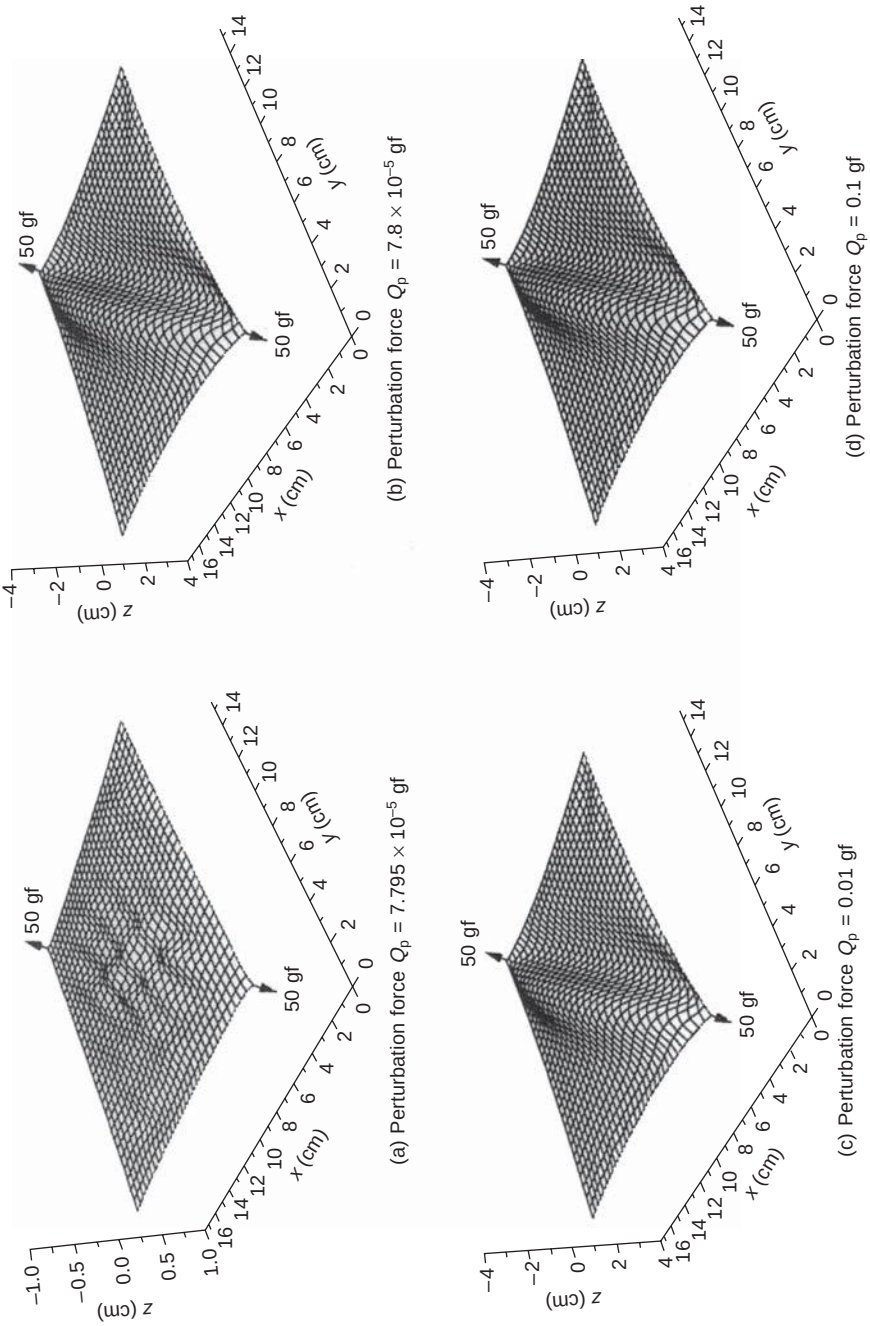

(a) Perturbation force $Q_p = 7.795 \times 10^{-5}$ gf

(b) Perturbation force $Q_p = 7.8 \times 10^{-5}$ gf

(c) Perturbation force $Q_p = 0.01$ gf

(d) Perturbation force $Q_p = 0.1$ gf

10.11 (a–h) Out-of-plane deformations of a fabric sheet under diagonal tension.

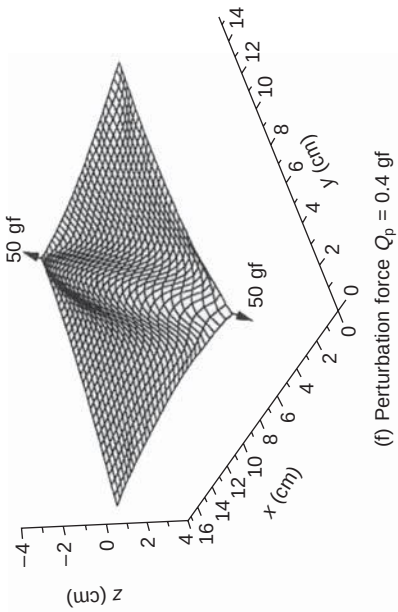

(e) Perturbation force $Q_p = 0.3$ gf

(f) Perturbation force $Q_p = 0.4$ gf

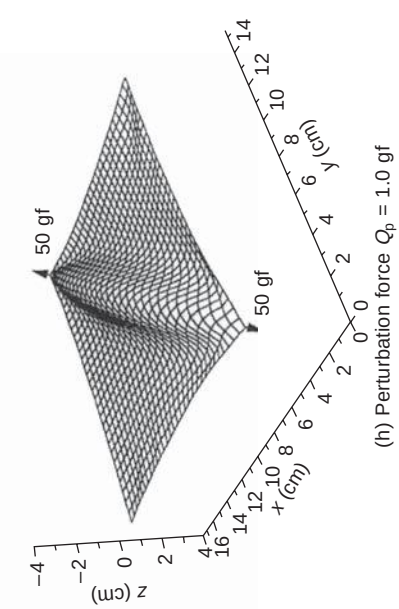

(g) Perturbation force $Q_p = 0.5$ gf

(h) Perturbation force $Q_p = 1.0$ gf

10.11 (cont.)

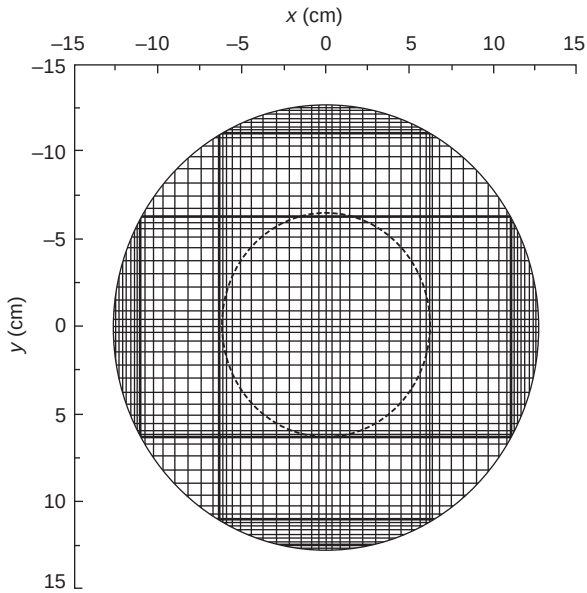

10.12 A grid scheme for fabric sheet A.

pedestal is 6.35 cm. A 65 × 65 non-uniform grid with 2365 nodes (or control volumes) was used in the simulation when the entire sheet was modelled. The grid is symmetric about the *x*- and *y*-axes, as shown in Fig. 10.12. The grid nodes which are in contact with the rigid pedestal were fixed in all directions.

Since both the geometry and the fabric material properties are doubly symmetric about the *x*- and *y*- (or warp and weft) axes, the deformed shape is expected to be doubly symmetric under fully idealised conditions (i.e. without any perturbation or initial imperfections). Consequently, a quarter section of the fabric sheet was first modelled with symmetric boundary conditions imposed along the two axes of symmetry. The same grid divisions as those used for a whole sheet model were adopted for the quarter section model, with a 33 × 33 grid. The drape shape predicted using this model features four curved folds (Fig. 10.13). It should be noted that Fig. 10.13, as well as all other figures, shows only the vertical projections of the drape shapes. It is believed that vertical projections can best illustrate the drape patterns, at least in terms of the number of waves and the degree of symmetry. Kang and Yu (1995) studied the same problem using the finite-element method, also employing a quarter section model. Their simulated deformed shapes together with their experimental shapes, both with four folds, are shown in Fig. 10.14 for comparison with the theoretical prediction.

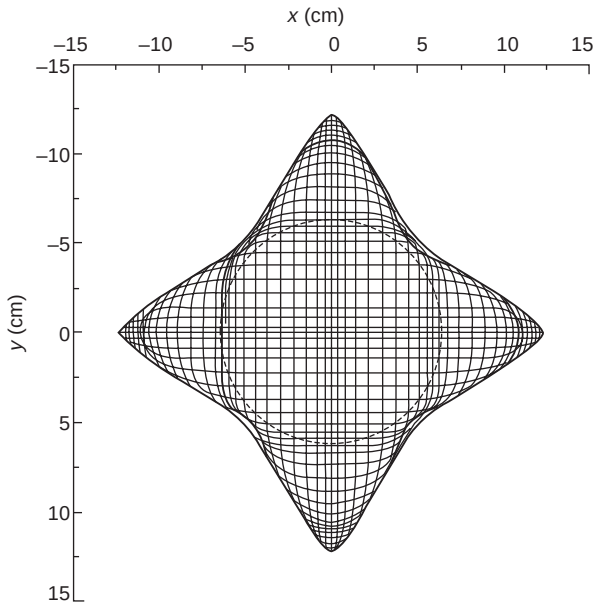

10.13 Doubly symmetric drape pattern of fabric sheet A.

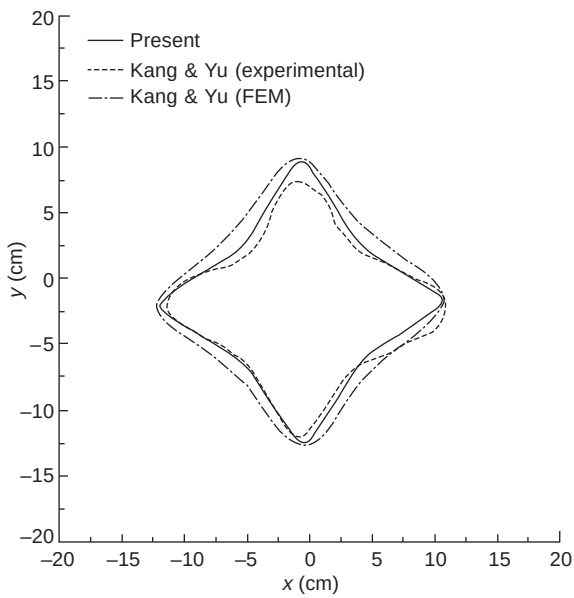

10.14 Comparison of doubly symmetric drape patterns of fabric sheet A.

It is clear from Fig. 10.14 that the present model presents a better fit with the experimental curve than that of Kang and Yu (1995). The simulated shape by Kang and Yu is too stiff as compared with the experimental shape. In addition, no other drape patterns were predicted or discussed in their study.

It is well known from simple experiments or daily experiences that the drape results of circular fabric sheets over circular pedestals are sensitive to any small perturbations or initial imperfections/deviations. Different drape patterns may appear in repeated experiments using the same fabric sheet on the same supporting pedestal. Studies on the buckling of thin shells show that the buckling and post-buckling deformations of shells are sensitive to initial imperfections and disturbances (Teng, 1996). As the drape deformations of circular fabric sheets are those of post-buckling deformations, it is expected that the final deformed pattern is sensitive to small perturbations or initial imperfections. This possibility has been briefly explored by Chen and Govindranaj (1995) for a tensioned square fabric sheet. The effect of small disturbances on the drape pattern of a circular fabric sheet is studied here in order to explain the multiplicity of drape patterns observed in experiments.

When the quarter section model was used, the doubly symmetric deformation pattern (Fig. 10.15) was ensured by imposing appropriate constraints along the axes of symmetry. When the whole fabric sheet was modelled using a 65×65 grid, the predicted drape pattern (Fig. 10.15a) featured six curved folds rather than four, and was asymmetrical about the original axes of symmetry. This asymmetric shape was obtained without applying any disturbance to destroy the double symmetry of the problem. This may appear surprising at first, but it should be realised that, although a bifurcation analysis was not carried out, the fabric sheet can deform into an asymmetrical shape through perturbations from numerical approximation and roundoff errors. The asymmetric drape is thus predicted to be the preferred shape if the sheet is not constrained during the deformation process.

So far two different drape patterns have been predicted for this fabric sheet without adding external perturbations. In order to find out whether other drape patterns exist for it, a small perturbation force was then applied to the fabric sheet during the simulation. The perturbation force used is a small concentrated force in the positive x-direction, applied at the point with the following initial co-ordinates: $x = 2.7$ cm and $y = 0$. Figures 10.15b–e show the drape patterns predicted with perturbation forces of different magnitudes. When the perturbation force is sufficiently small ($Q_p = 5 \times 10^{-5}$ gf), the drape shape retains the six-fold pattern (Fig. 10.15b). However, when Q_p reaches 1×10^{-4} gf or higher, the fabric sheet exhibits other drape patterns all with seven curved folds (Figs 10.15c–e). Drape patterns with seven curved folds appear to be more stable than other patterns since an increase in the perturbation force from 1×10^{-4} gf to 0.01 gf cannot change the number of folds.

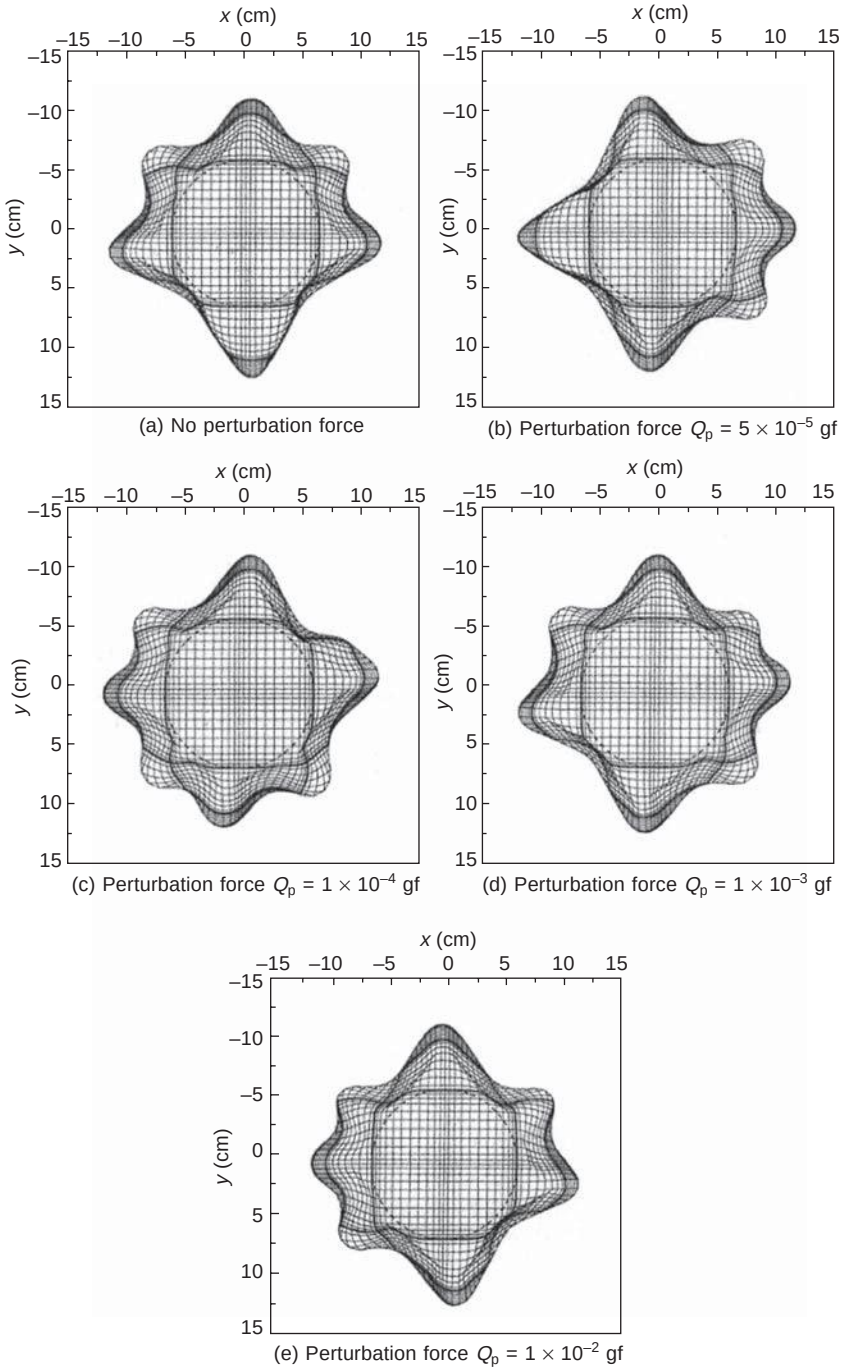

10.15 Drape pattern of fabric sheet A with a horizontal perturbation force.

10.6.2 Drape behaviour of a circular fabric sheet B

The sheet made of fabric B, referred to as fabric sheet B, has a radius of 15 cm and is supported by a pedestal of radius 9 cm. When the whole fabric sheet was modelled, a 69×69 division grid with 2649 nodes was adopted. The simulation procedure is similar to that for fabric sheet A discussed above. Figures 10.16a–e show the drape patterns predicted with a horizontal perturbation force of different magnitudes in the positive x-direction. The concentrated perturbation force was applied at the point with initial co-ordinates $x = 15$ cm and $y = 0$.

When the whole fabric surface was used in the simulation without a perturbation force, the deformed pattern was predicted to be unsymmetrical with nine folds instead (Fig. 10.16a). A similar deformed pattern with nine folds was found when a horizontal perturbation force $Q_p = 5 \times 10^{-5}$ gf was applied (Fig. 10.16b). Moreover, when Q_p reaches 1×10^{-4} gf, ten folds are present in the drape pattern (Fig. 10.16c). When $Q_p = 1 \times 10^{-3}$ gf, the deformed shape exhibits a different nine-fold pattern (Fig. 10.16d). When a relatively high Q_p of 1×10^{-2} gf was applied, the deformed shape returns to an eight-fold pattern (Fig. 10.16e) which is much closer to the doubly symmetric pattern.

The drape patterns of the fabric sheet B are seen to have eight to ten curved folds (Fig. 10.16), with nine-fold patterns appearing more often than others. With a relatively high perturbation force, the drape shape usually features eight folds, and the chance of seeing a ten-fold pattern is relatively small. Gan *et al*. (1995) studied the same fabric drape problem using the finite-element method and predicted an eight-fold drape pattern only for this fabric sheet. They also pointed out that in experiments the drape pattern of this fabric sheet had six to eight folds. This experimental observation does not match the numerical results presented above. This does not mean, however, that the numerical approach is flawed in any sense, as the discrepancy could have been caused by some or all of the many possible factors including deviations in shape, material properties and experimental conditions from those assumed in the analysis. The important fact that has been demonstrated is that small disturbances can change the drape patterns significantly.

10.7 Contact drape simulation of woven fabrics and garments

10.7.1 Contact determination algorithm

The two main methods adopted for the treatment of contact problems in non-linear finite-element analysis are the penalty method and the Lagrangian multiplier method (Crisfield, 1997). The penalty method is closely related to techniques which attempt to introduce a high stiffness for the contact region.

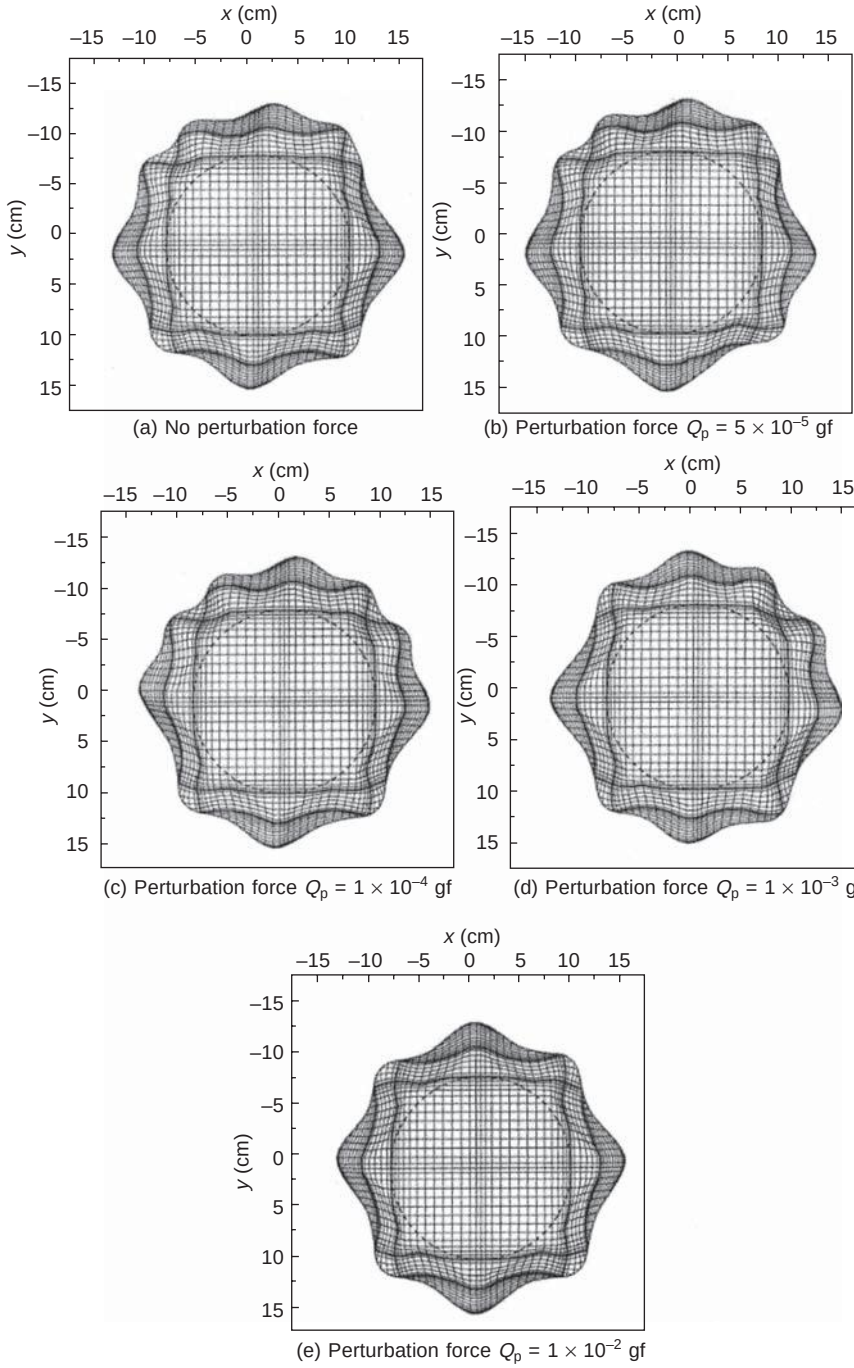

10.16 Drape patterns of fabric sheet B with a horizontal perturbation force.

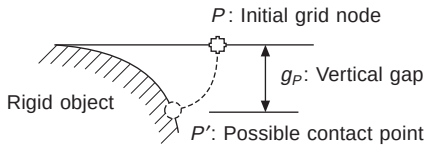

10.17 Two-dimensional case of fabric contact with rigid object.

However, in this approach, the magnitude of the penalty constant may affect the convergence of the iterative procedure. An excessively large constant can cause divergence. On the other hand, in the Lagrangian multiplier method, the number of equational unknowns must be increased, which leads to complexity and difficulty in computer implementation. In this study, a simpler but effective approach for dealing with the contact process between a cloth falling from an initial flat position and a rigid object is developed. This is described below.

Before deformation, the cloth is fully flat. The vertical distances between the initial positions of all grid nodes and their possible contact points (if any) are then calculated. The calculation is based on the plausible assumption that the in-plane stretching of the cloth is very small and an initial control volume retains its original surface area during the process of draping. Figure 10.17 shows a two-dimensional case of such a contact problem. During the numerical iteration, if the current increment makes the total vertical displacement of a grid node exceed its vertical gap, the condition that the vertical displacement increment is equal to the difference of the vertical gap and the displacement is imposed upon the grid node. As a result, the grid node is pulled back vertically. In this approach, there is no need to increase the number of equational unknowns or introduce large penalty constants which may cause numerical convergence problems. Therefore, the approach is rather simple and easy for computer implementation with the finite-volume method. Through the numerical simulations described in the next section this contact determination approach is proved to be both valid and efficient.

10.7.2 Simulation of contact drape

A number of numerical simulations of fabric pieces and simple garments are presented in this section. We start with the drape prediction of a square piece of full polyester fabric and a piece of pure wool fabric over a round rod; then a square piece of pure wool fabric and a piece of pure cotton fabric draped over a sphere are analysed. Finally the simulation results for a wool and a cotton skirt draped over and in contact with a synthetic body form from their initial flat positions are presented. The three types of fabric materials used here, namely polyester, wool and cotton materials, have been experimentally studied by Deng (1994) and Kang and Yu (1995), as listed in Table 10.3.

Table 10.3 Material properties of fabrics

Property	Notation	Polyester	Wool	Cotton
Tensile rigidity	E_{warp}	235724.7	1118.2	2531.6
(gf/cm)	E_{weft}	145680.8	759.5	1413.5
Bending rigidity	D_{warp}	0.322	0.083	0.068
(gf cm^2/cm)	D_{weft}	0.199	0.063	0.030
Shearing rigidity (gf/cm)	G	2800.0	41.8	250.7
Weight (gf/cm^2)	w	0.01715	0.019	0.0095
Thickness (cm)	h	0.0254	0.0593	0.0469

1 gf = 0.0098 N

10.7.2.1 Square fabric pieces draped over a round rod

Considering a fabric piece with the dimensions 20 cm × 20 cm, the problem involves the draping of the fabric piece on a round rod of radius 2.5 cm, which is placed diagonally under it. The simulation was first carried out for the polyester fabric material as the same problem was experimentally studied and numerically predicted using the finite-element method by Deng (1994). In his study, only bending rigidities in the warp and weft directions were experimentally obtained, while the tensile rigidities were derived from the bending rigidities using the approach in the classical plate/shell theory. In his finite-element analysis, however, Deng (1994) used an isotropic and geometrically non-linear shell element model, so only the warp-direction rigidities were actually included in the numerical simulation. The shear modulus was simply set equal to the tensile modulus, considering that the shear modulus showed relative insensitivity to the drape deformations, and the Poisson's ratio was set to 0.3. We presume that the fabric material is assumed to be linear elastic and orthotropic. The material properties in both the warp and weft directions, as listed in the third column of Table 10.3, were all included in the numerical simulation. The shear rigidity of the fabric was set to be 2800 gf/cm which is about 2 % of the weft-direction tensile rigidity, considering that the shear rigidity of the fabric is in general much smaller than the tensile rigidities. The effect of the Poisson's ratio was neglected in all simulations as mentioned earlier. A uniform grid of 33 × 33 nodes (or control volumes), as shown in Fig. 10.18, was adopted in the simulation.

Figure 10.19a shows the three-dimensional drape shape of this polyester fabric. Table 10.4 lists the three deformed co-ordinates of corner point A and compares them with the experimental data and those of the finite-element method of Deng (1994). It is seen from Table 10.4 that the predicted co-ordinates closely match the experimental results.

In order to compare the contact drape behaviour of different fabric materials, a simulation was also carried out for a wool fabric sheet of the same size

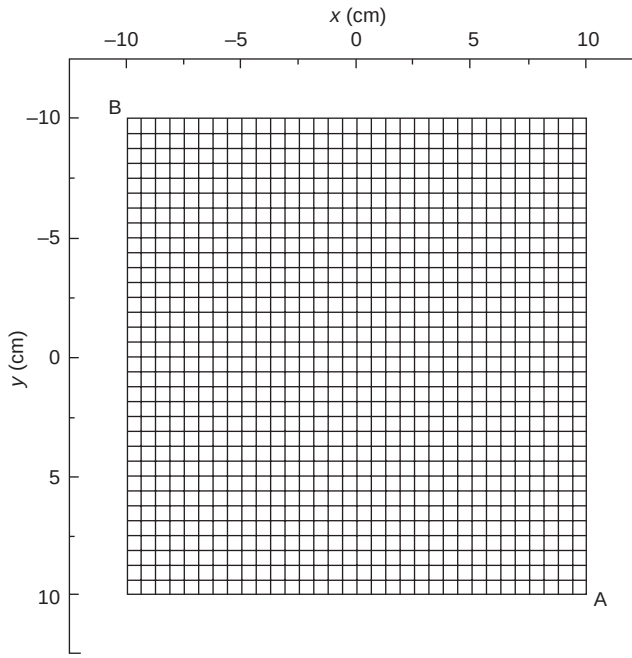

10.18 A uniform grid scheme for square fabric pieces draped over a rod.

draped over the same round rod. The simulated drape shape of the fabric is shown in Fig. 10.19b. The wool fabric piece is seen to exhibit a greater degree of draping than the polyester fabric counterpart. The calculated vertical co-ordinate of the corner point A (or B) of the former is larger than that of the latter and the corresponding horizontal co-ordinates of the former are smaller than those of the latter (Fig. 10.19). This demonstrates that the wool fabric has a better drapeability than the polyester fabric.

Both the above simulations were achieved on a Pentium® II/266 personal computer. The computational times required for the two simulations, are only 3 hours and 10 minutes for the polyester fabric and 28 minutes for the wool fabric. This shows that the drape simulation for the wool fabric with a greater drapeability is much faster than that for polyester fabric with stiffer mechanical properties. Much faster simulations can be achieved if a more powerful PC or workstation is used. Although precise comparison in computer time with other methods is not possible as different grid schemes, different computers and other variables are involved, the efficiency of the present method together with the proposed contact determination approach is easily demonstrated by noting that a draping simulation using a 51×51 grid requires one week on an IBM RS/6000 workstation.

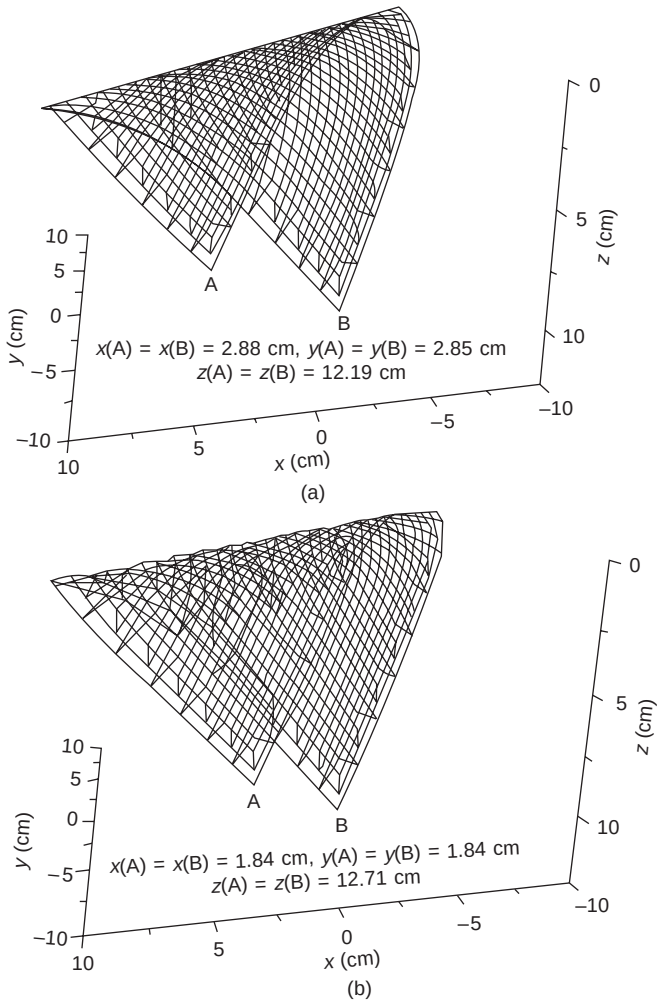

10.19 Drape shapes of square fabric pieces over a rod: (a) polyester fabric; (b) wool fabric.

Table 10.4 Deformed co-ordinates of point A of the polyester fabric piece

Co-ordinates of points A	***x* (cm)**	***y* (cm)**	***z* (cm)**
Initial co-ordinate	10	10	0
Theoretical prediction	2.88	2.85	12.19
Finite element prediction (Deng, 1994)	2.70	2.70	12.56
Experimental result (Deng, 1994)	3.27	3.27	12.25

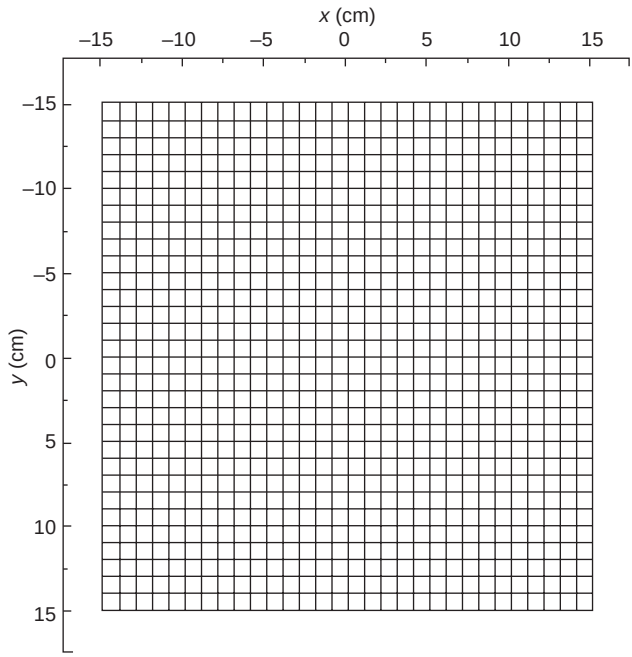

10.20 A uniform grid scheme for fabric pieces draped over a sphere.

10.7.2.2 Square fabric pieces draped over a sphere

In order to further investigate the validity and capacity of the present method and further compare the drapeability of different fabric materials, two square pieces of fabric 30 cm × 30 cm in size, one of wool material and one of cotton, concentrically draped over a sphere of 5 cm in radius were also analysed. Their mechanical properties are listed in Table 10.3. Both fabric pieces were modelled by a uniform grid of 31 × 31 nodes, as shown in Fig.10.20. The predicted drape shapes of the two fabric pieces are given in Figs 10.21a and b. Both shapes feature four main folds with smaller curved wrinkles between them. The wool fabric piece, however, is seen to exhibit a significantly greater degree of draping than the cotton fabric. The cotton fabric appears to be relatively stiff and does not drape so thoroughly over the sphere as the wool fabric does. This verifies the good drapeability of the wool fabric material in comparison with the cotton material.

The drape simulation of the two fabric pieces was again carried out using a finer grid scheme of 51 × 51 nodes, the results of which are shown in Fig. 10.22. The overall drape shapes of the two fabric pieces are similar to those presented in Fig. 10.21, demonstrating the reliability of the present method and the proposed contact determination approach. The northeast and southeast

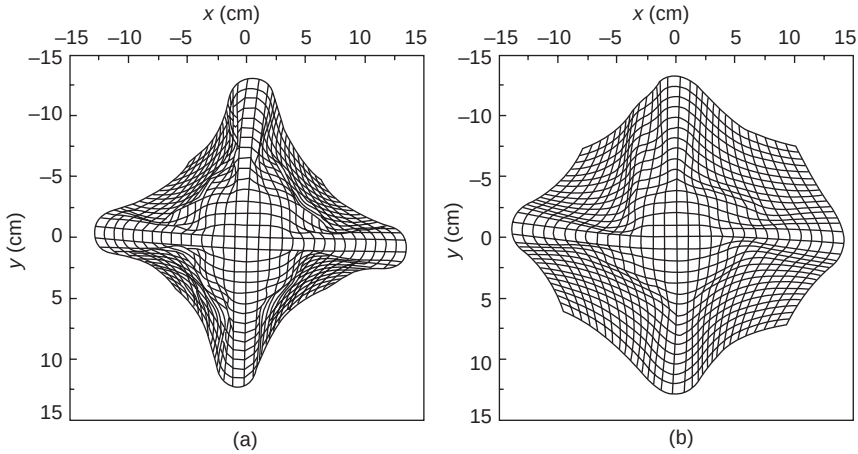

10.21 Drape shapes of square fabric pieces over a sphere: (a) wool fabric; (b) cotton fabric.

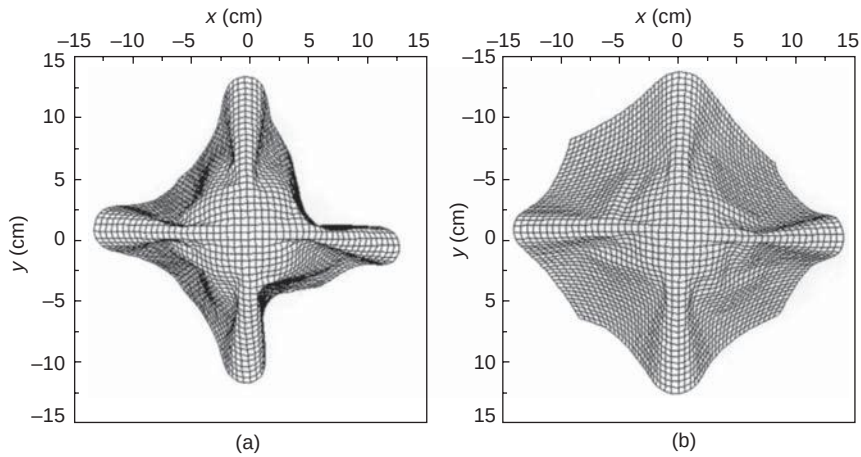

10.22 Drape shapes of square fabric pieces over a sphere using a finer grid: (a) wool fabric; (b) cotton fabric.

corners of the two fabric pieces in Fig. 10.22, however, undergo greater drape deformations than those presented in Fig. 10.21. This demonstrates that, using the present method, a fabric piece modelled by a coarse grid generally appears stiffer than one modelled by a finer grid. More importantly, the drape shapes predicted using a finer grid contain more detailed information of deformations including small curved wrinkles as shown in Fig. 10.22, particularly for the cotton fabric piece (Fig. 10.22b).

Naturally, the better results with a finer grid come with higher computational cost. The simulation of the drape shape of the wool fabric piece using a

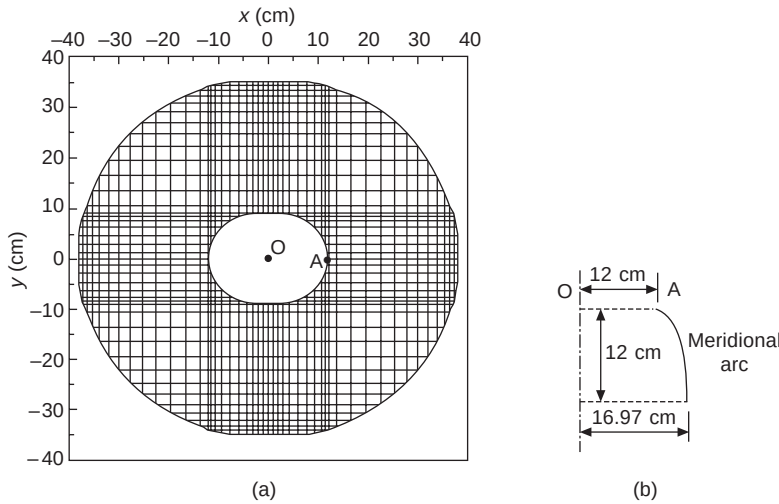

10.23 Modelling of a skirt attached to a human body: (a) non-uniform grid scheme; (b) meridional profile of body form.

31 × 31 grid as shown in Fig. 10.23a requires only 1 hour and 10 minutes, while the corresponding simulation using a 51 × 51 grid as shown in Fig. 10.22a requires 10 hours and 14 minutes, both on a Pentium® II/266 personal computer. Therefore, the choice of a grid needs to strike a balance between accuracy and computational time. For the cotton fabric, the simulations of the drape shapes as shown in Fig. 10.21b require 1 hour and 12 minutes and 17 hours and 10 minutes respectively. A comparison between the computer times required for the simulations of the wool and cotton fabric pieces again confirms that drape simulation is faster for fabric materials with a better drapability/softer mechanical properties, using the full Newton–Raphson iteration method with line searches as adopted here.

10.7.2.3 Skirts attached to a body form

The problem of a skirt draping over and interacting with a synthetic body form is considered here. The pre-drape configuration of the skirt is a flat cloth. The circumference of the body form at any vertical position was obtained by moving all points of the circumference at the top of the skirt (the inner boundary of the mesh shown in Fig. 10.23a) in the normal direction by the same amount. The distance between two corresponding points on any two circumferences was determined by the meridional profile adopted, which only had to be specified at one point around the circumference. Figure 10.23b shows the circular arc meridional profile used in the simulations described below.

Figure 10.23a shows the finite-volume grid scheme of the flat cloth used in the simulation. The non-uniform grid was used to suit the outer and inner boundaries of the skirt cloth. Two fabric materials, pure wool and pure cotton, with their mechanical properties as given in Table 10.3, were considered in the simulations. Figure 10.24 shows the three-dimensional drape shapes of the two skirts obtained using the present method, while Fig. 10.25 shows the corresponding vertical projections of the final shapes. The outlines of the two vertical projections are given in Fig. 10.26a and b, respectively. These figures were all produced by directly joining the calculated positions of all

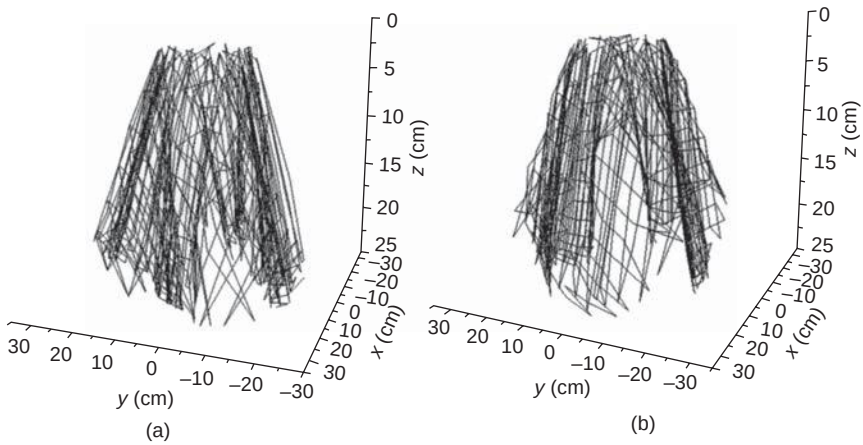

10.24 Three-dimensional drape shapes of skirts attached to a synthetic body form: (a) wool fabric; (b) cotton fabric.

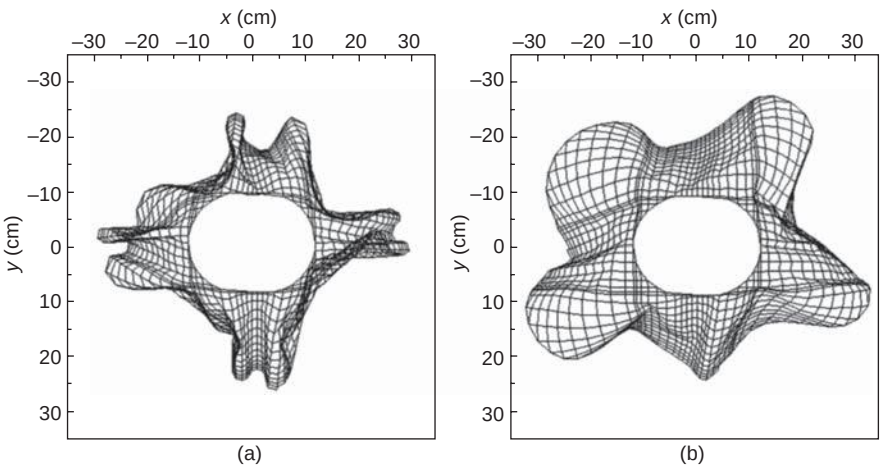

10.25 Vertical projections of skirts attached to a synthetic body form: (a) wool fabric; (b) cotton fabric.

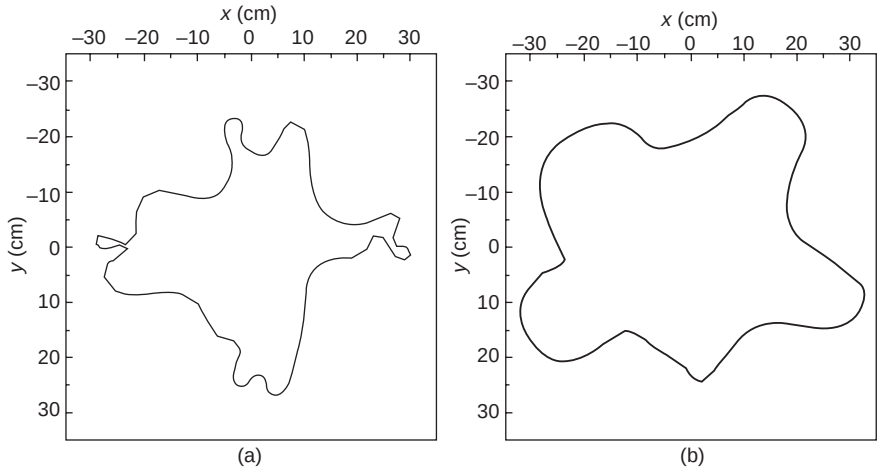

10.26 Outlines of vertical projections of skirts: (a) wool fabric; (b) cotton fabric.

grid nodes along the warp and weft directions by a straight line. Enhanced images with better visual effect can be obtained by using some curve- or surface-fitting plot software, which should be considered in future studies. The simulations for the wool and the cotton skirts took 2 hours and 31 minutes and 5 hours and 47 minutes on a Pentium® II/266 personal computer, respectively.

It is clear from Figs 10.24–26 that the two skirts exhibit complicated drape surfaces characterised by curved folds and wrinkles of various sizes. Although the initial geometry, material properties and boundary conditions of the two skirts are doubly symmetric about the *x*- and *y*-axis (Fig. 10.23), the deformed shapes do not retain the original symmetry again. Since bifurcation/buckling phenomena can occur during the process of draping, the skirts can deform into a preferred unsymmetrical shape through perturbations from numerical approximation and roundoff errors (Hu and Chung, 1998). It is seen from the comparison of parts (a) and (b) in Figs 10.24–26 that the wool skirt shows a greater degree of draping and a more complex drape shape than the cotton skirt. This again demonstrates the good drapeability of the wool fabric material studied here. Although there are no other available theoretical or experimental results for comparison with the present predictions, the results here do give realistic and reasonable shapes. This gives us confidence in the capability of the present method to model complicated contact drape problems of various clothing products including garments. It is thus suitable for use in the development of powerful clothing CAD systems.

10.8 Three-dimensional skirt simulation by using B-spline surface

It is well known that space spline surface has wide applications, including the modelling of objects such as robots, the design of cars, ships, aeroplanes, and computer simulation of virtual animals and humans. The B-spline paradigm for modelling smooth surfaces is limited by the requirement that the control point mesh must be organised as a regular rectangular structure. Ignoring this requirement by collapsing the control mesh edges leads to surfaces with ambiguous surface normal and degenerated parameterisation (Peirce, 1937). Many approximation approaches have been considered for modelling surfaces of arbitrary topological type by smoothly approximating an irregular control mesh. The limitation of this polishing method is that it does not satisfy the interpolation condition. A local interpolation method has also been discussed for constructing a piecewise smooth interpolation space surface (Hearle *et al.*, 1969, 1980; Skelton, 1974; Barker *et al*., 1985, 1986, 1987). A smooth piecewise quartic surface was constructed with triangular Bézier patches by Hearle *et al.* (1980). A cubic interpolation scheme for constructing GC^1 surface over space triangles and space quadrangles has also been presented. These methods are based on increasing the free-degrees of each surface patch by using increasing polynomial order or refinement of space mesh. In general, surface degree is not less quartic. In applying these methods, surface shapes depend on determination of parameter and estimation of gradient. It is concluded that local polynomial interplant generally produces unsatisfactory shapes (Kawabata, 1980a, b).

In this section, we consider an application of smooth interpolation space surface in clothing simulation. Combining both the fabric frame and the B-spline method generates a trimming B-spline interpolation surface over space mesh. The advantages of this technique are simplicity, efficiency and ease of display. The surface, as a whole parameter surface, is smooth and interpolates space mesh points.

The interpolation surface algorithm takes a space mesh as input. The mesh is extended to a regular rectangular mesh so that it fits into the product B-spline surface representation. Next, a B-spline surface is generated for interpolating the rectangular mesh vertices in which the boundary curves divide the interpolation surface into two parts, the initial and the extended surface. B-spline basis functions are chosen with equidistant knots and are bi-cubic. To compute the control points of the B-spline, it is necessary to solve the linear equation system which is recursively divided into small subsystems. The three-dimensional skirt surface is constructed by trimming the rectangular B-spline surface along with the boundary curves. Finally, a three-dimensional texture mapping technique is used to put the image texture on the skirt surface.

10.8.1 Background

This section gives a brief review of B-spline curve and surface. Some details can be found in Kawabata (1980), Oloffson (1967), Skelton and Schoppee (1976).

10.8.1.1 B-spline curve and surfaces

Given $m + p - 1$ space points $\{p_i \in R^3: i = 1, 2, \ldots, m + p - 1\}$ and a partition of the interval $[0, p]$, $s_1, s_2, \ldots, s_{2m+p-1}$, a degree m B-spline curve is defined as

$$p(s) = \sum_{i=1}^{m+p-1} p_i N_{i,m}(s) \quad s \in [0, p],$$

where

$$N_{i,1}(s) = \begin{cases} 1 & s_i \le s < s_{i+1} \\ 0 & \text{other} \end{cases}$$

and

$$N_{i,m}(s) = \frac{s - s_i}{s_{i+m-1} - s_i} N_{i,m-1}(s) + \frac{s_{i+m} - s}{s_{i+m} - s_{i+1}} N_{i+1,m-1}(s) \quad m > 1$$

are the basis function of B-spline.

The $m \times n$ B-spline surface is the tensor product of a two direction B-spline curve. Given space points $\{p_{ij} \in R^3 : i = 1, 2, \ldots, m + p - 1, j = 1, 2, \ldots, n + q - 1\}$ and two partitions, $s_1, s_2, \ldots, s_{2m+p-1}$, $t_1, t_2, \ldots, t_{2n+q-1}$ a degree $m \times n$ B-spline surface is defined as

$$p(s, t) = \sum_{i=1}^{m+p-1} \sum_{j=1}^{n+q-1} p_{ij} N_{i,m}(s) N_{j,n}(t) \quad (s, t) \in [0, p] \times [0, q].$$

B-spline surfaces, as a kind of parameter surface form, are widely applied in space surface representation, geometric design and object modelling. Low degree B-spline surface can be applied to surface rendering, shape control and collision detection.

10.8.1.2 B-spline interpolation

The B-spline interpolation means the construction of a B-spline surface so that it passes through the given space points. This can be described as follows. Given space points $\{Q_{ij} \in R^3 : i = 0, 1, \ldots, m + p - 1, j = 1, 2, \ldots, n + q - 1\}$ and two partitions, $s_1, s_2, \ldots, s_{2m+p-1}$, $t_1, t_2, \ldots, t_{2n+q-1}$, a B-spline surface $p(s)$ with given knots can be constructed so that the surface satisfies

the interpolation condition, that is

$$p(s_k, t_l) = \sum_{i=1}^{m+p-1} \sum_{j=1}^{n+q-1} p_{ij} N_{i,m}(s_k) N_{j,n}(t_l) = Q_{kl}$$

with

$$k = 0, 1, \ldots, m + p - 1, \; l = 1, 2, \ldots, n + q - 1$$

To compute the control points of the surface, it is necessary to solve a $m + p - 1 \times n + q - 1$ linear equation system. In fact, it can be translated to solve curve interpolation recursively. This can be represented as:

$$\begin{aligned} p(s, t) &= \sum_{i=1}^{m+p-1} \sum_{j=1}^{n+q-1} p_{ij} N_{i,m}(s) N_{j,n}(t) \\ &= \sum_{j=1}^{m+q-1} R_j(s) N_{j,n}(t) \\ &= \sum_{i=1}^{m+p-1} G_i(t) N_{i,m}(s). \end{aligned}$$

10.8.1.3 Texture mapping

Texture in graphics is an illumination function. It can be defined in both forms – mathematical model and image. This section adopts the latter. Let T be an $M \times N$ digital image. Divide the texture space into an $M \times N$ mesh and define a map from digital image to mesh vertices. The texture value in the mesh vertex takes the corresponding image value. The texture value inside the mesh can be computed by using interpolation methods. This defines a texture by digital image. Texture mapping is the process of building a mapping function from texture space to object surface. When computing light brightness in an illumination model, diffuse reflection shininess takes the texture function value.

10.8.2 Mesh extension

The three-dimensional skirt data come from a drape simulation computed by using a finite-volume method. It is deformed from a plane mesh. Because this mesh is not rectangular, it is necessary to extend the mesh to a rectangular one in order to construct an interpolation B-spline surface. This means adding some data to the original mesh along with its boundary. These three-dimensional space points are computed one by one from the boundary to the outside so that the whole mesh has a smooth shape (Fig. 10.27). It can be represented as follows.

If the extension point is connected with the boundary points in the vertical

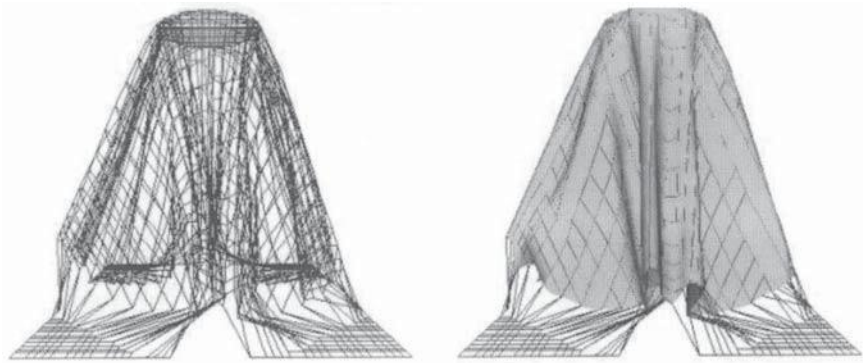

10.27 Extension mesh and trimming surface.

and horizontal directions, the point is set to be a linear combination of the four points that are connected in the two directions. If the extension point is connected with the boundary points in one direction, the point is set to be a linear combination of the two points that are connected in that direction.

10.8.3 B-spline surface interpolation

The extension rectangle mesh consists of 47 rows and 41 columns. The inside and outside boundaries are made up of 45 and 117 points respectively. For the extension rectangle mesh, we choose a bi-cubic B-spline surface with equidistant knots. The knots are the following:

- knots for parameter S:

  (0.0, 0.0, 0.0, 0.0, 1.0, 2.0, . . . , 42.0, 43.0, 44.0, 44.0, 44.0, 44.0)

- knots for parameter T:

  (0.0, 0.0, 0.0, 0.0, 1.0, 2.0, . . . , 36.0, 37.0, 38.0, 38.0, 38.0, 38.0)

  Let

  p_{ij}, $i = 1, 2, \ldots, 47$, $j = 1, 2, \ldots, 41$

  be the rectangle mesh points. The parameter interpolation points are chosen as:

- i-th column parameter points: $0, s_1^i, 1, 2, \ldots, 42, 43, s_2^i, 44$
- j-th row parameter points: $0, t_1^i, 1, 2, \ldots, 36, 37, t_2^i, 38$

  where

$$s_1^i = \frac{\| p_{i0} - p_{i1} \|}{\| p_{i0} - p_{i1} \| + \| p_{i1} - p_{i2} \|},$$

$$s_2^i = 44 - \frac{\| p_{i47} - p_{i46} \|}{\| p_{i47} - p_{i46} \| + \| p_{i45} - p_{i46} \|}$$

$$t_1^i = \frac{\| p_{0j} - p_{1j} \|}{\| p_{0j} - p_{1j} \| + \| p_{1j} - p_{2j} \|},$$

$$t_2^i = 38 - \frac{\| p_{41j} - p_{40j} \|}{\| p_{41j} - p_{40j} \| + \| p_{39j} - p_{40j} \|}$$

$i = 1, 2, \ldots, 41, j = 1, 2, \ldots, 47$

The B-spline parameter surface $P(s, t)$ defined on $[0,44] \times [0,38]$ is determined by the interpolation condition.

$$P(s_i, t_j) = p_{ij},\ i = 1, 2, \ldots, 47, j = 1, 2, \ldots, 41$$

10.8.4 Trimming surface

The previous section shows the construction of an interpolation B-spline surface for an extension mesh. To generalise the interpolation surface of original mesh, it is necessary to determine the boundary curves on the interpolation surface. A method of representing the boundary curves is to determine the parameter curves in the parameter field of the previous interpolation B-spline surface so that its mapping curves in the B-spline function are the boundary curves of original mesh. The following presents the construction of a precise representation of the boundary curves in the parameter field of the previous interpolation B-spline surface.

The B-spline surface interpolates all vertices of the extension mesh, including the boundary vertices of the original mesh. The parameter points of the boundary vertices can be determined in the parameter field from the interpolation parameter points. Two boundary curves can be computed by using a method similar to the one introduced in the previous section. A cubic B-spline curve with equidistant knots is chosen. The knots are the following:

- parameter knots for outside boundary curve:

  (0.0, 0.0, 0.0, 0.0, 1.0, 2.0, . . . , 112.0, 113.0,114.0, 114.0, 114.0, 114.0)

- parameter knots for inside boundary curve:

  (0.0, 0.0, 0.0, 0.0, 1.0, 2.0, . . . , 40.0, 41.0, 42.0, 42.0, 42.0, 42.0)

10.8.5 Texture mapping for the skirt

For the skirt surface, using a map from digital image field to parameter field of the surface can represent the texture mapping. This map can be constructed

by a map from image field $M \times N$ to the extension surface parameter field $(0,38) \times (0,42)$. To obtain texture mapping with different repeats in row and column, we combine a new large image as a texture image by iteratively combining the repeat image in row and column directions. Figure 10.28 is the texture mapping of the skirt with a single repeat and with 6×6 repeats. The size of a single repeat texture image is 256×256.

10.28 The texture mapping of skirt with a single repeat and 6×6 repeats. The size of single repeat texture image is 256×256: (a) skirt surface; (b)–(g) texture mapping of skirt with a single repeat; (h)–(m) texture mapping of skirt with 6×6 repeats.

(e)

(f)

(g)

(h)

(i)

(j)

10.28 (cont.)

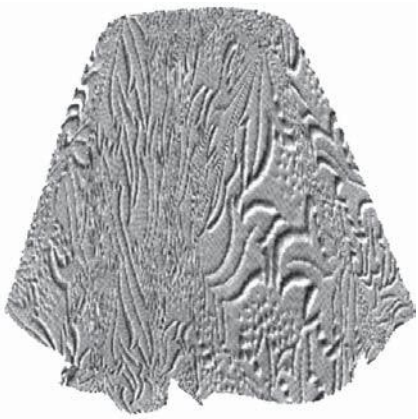

(k)

(l)

(m)

10.28 (cont.)

10.8.6 Summary

This part of the chapter presents a scheme for constructing a three-dimensional skirt surface with special texture. The scheme is an application of B-spline and texture mapping techniques to clothing modelling. Beginning with an initial three-dimensional skirt mesh, an extended regular rectangular mesh is constructed which includes the initial mesh. A B-spline surface is generated for interpolating the rectangular mesh vertices in which the boundary curves divide the interpolation surface into two parts, the initial and the extended

surface. Using B-spline curve in parameter field of B-spline interpolation surface represents the two boundary curves. They are determined by interpolating the boundary vertices. The three-dimensional skirt surface is constructed by trimming the rectangular B-spline surface along with the boundary curves. Finally, a three-dimensional texture mapping technique is used to put the image texture on the skirt surface. The texture size is changeable with repeating.

10.9 References

Barker R *et al* (1985 May, 1986 February & 1987 March), *Reports to North Carolina State University*, Raleigh, North Carolina 27695–8301, Kawabata Consortium, School of Textiles, North Carolina State University.

Chen B and Govindaraj M (1995), A physical based model of fabric drape using flexible shell theory, *Text Res J*, **65**(6), 324–330.

Crisfield, M (1997), *Non-linear Finite Element Analysis of Solids and Structures*, Volume II: Advanced Topics, Chichester, John Wiley & Sons.

Deng S (1994), *Nonlinear Fabric Mechanics Including Material Nonlinearity, Contact and an Adaptive Global Solution Algorithm* (Doctoral Dissertation, North Carolina State University, Raleigh, N C.

Dhande S G, Rao P V M and Moore C L (1993), Geometric modelling of draped fabric surfaces, *Graphics, design and visualization (Proc Int Conf on Computer Graphics)*, S P Mudur and S N Pattanaik (eds), Bombay, Jaico Publishing House, 173–180.

Gan L, Ly Ng and Steven G P (1995), A study of fabric deformation using non-linear finite elements, *Text Res J*, **65**(11), 660–668.

Hearle J W S, Grosberg P and Backer S (1969), *Structural Mechanics of Fibres, Yarns, and Fabrics: vol I*, New York, Wiley-Interscience, 340.

Hearle J W S, Thwaites J J and Amirbayat J (1980), *Mechanics of Flexible Fibres Assemblies (NATO Advanced Study Institute Series: E, Applied Sciences No 38*), The Netherlands, Alpen aan den Rijn, Sijthoff and Noordhoff.

Hu J L and Chung S P (1998), Investigation of drape behaviour on woven fabrics with seams, *Text Res J*, **68**(12), 913–919.

Kang T J and Yu W R (1995), Drape simulation of woven fabric by using the finite-element method, *J Text Inst*, **86**(4), 635–648.

Kawabata S (1975), *The Standardization and Analysis of Hand Evaluation*, Osaka, hand evaluation and standardization committee of the Textile Machinery Society of Japan.

Kawabata S (1980), Examination of effect of basic mechanical properties of fabric hand, in *Mechanics of Flexible Fibre Assemblies (NATO Advanced Study Institute Series: E, Applied Sciences No 38)*, Hearle J W S, Thwaites J J and Ambirbayat J (eds), The Netherlands, Alpen aan den Rijn, Sijthoff and Noordhoff 14–18.

Kawabata S (1980, July), *Standardisation and Analysis of Hand Evaluation*, *2nd edition Osaka*, the Textile Machinery Society of Japan.

Kim J (1991), *Fabric Mechanics Analysis Using Large Deformation Orthotropic Shell Theory* (Doctoral Dissertation, North Carolina State University, Raleigh, NC).

Oloffson B (1967), Study of inelastic deformations of textile fabrics, *J Text Inst*, **58,** 221.

Peirce F T (1937), The geometry of cloth structure, *J Text Inst*, **28,** 45–96.

Skelton J (1974), Frictional effects in fibrous assemblies, *Text Res J*, **44**, 746–752.
Skelton J and Schoppee M M (1976), Frictional damping in multicomponent assemblies, *Text Res J*, **46**, 661–667.
Teng J G (1996), Buckling of thin shells: recent advances and trends, *Appl Mech Rev ASME*, **49**(4), 263–274.